

Quantum state-dependent anion–neutral detachment processes

Cite as: J. Chem. Phys. **156**, 094304 (2022); <https://doi.org/10.1063/5.0082734>

Submitted: 17 December 2021 • Accepted: 08 February 2022 • Accepted Manuscript Online: 08 February 2022 • Published Online: 01 March 2022

 Saba Zia Hassan, Jonas Tauch, Milaim Kas, et al.



View Online



Export Citation



CrossMark

ARTICLES YOU MAY BE INTERESTED IN

The dynamics of CO production from the photolysis of acetone across the whole $S_1 \leftarrow S_0$ absorption spectrum: Roaming and triple fragmentation pathways

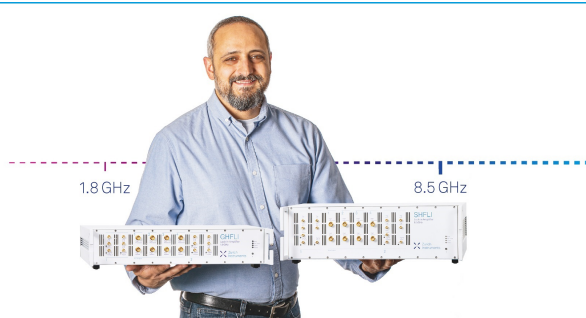
The Journal of Chemical Physics **156**, 094303 (2022); <https://doi.org/10.1063/5.0080904>

Do not forget the Rydberg orbitals

The Journal of Chemical Physics **156**, 100901 (2022); <https://doi.org/10.1063/5.0084574>


Optimal control of photodissociation of phenol using genetic algorithm

The Journal of Chemical Physics **156**, 094305 (2022); <https://doi.org/10.1063/5.0081282>



Trailblazers. New

Meet the Lock-in Amplifiers that measure microwaves.

 Zurich Instruments

[Find out more](#)

Quantum state-dependent anion-neutral detachment processes

Cite as: J. Chem. Phys. 156, 094304 (2022); doi: 10.1063/5.0082734

Submitted: 17 December 2021 • Accepted: 8 February 2022 •

Published Online: 1 March 2022



View Online



Export Citation



CrossMark

Saba Zia Hassan,^{1,a)} Jonas Tauch,¹ Milaim Kas,^{2,3} Markus Nötzold,⁴ Roland Wester,^{4,b)}
and Matthias Weidemüller^{1,c)}

AFFILIATIONS

¹Physikalisches Institut, Ruprecht-Karls-Universität Heidelberg, 69120 Heidelberg, Germany

²Deutsches Elektronen-Synchrotron (DESY), 22607 Hamburg, Germany

³Department of Mathematics, Universität Hamburg, 20146 Hamburg, Germany

⁴Institut für Ionenphysik und Angewandte Physik, Universität Innsbruck, 6020 Innsbruck, Austria

^{a)}Author to whom correspondence should be addressed: hassan@physi.uni-heidelberg.de

^{b)}Electronic mail: roland.wester@uibk.ac.at

^{c)}Electronic mail: weidemueLLer@uni-heidelberg.de

ABSTRACT

The detachment loss dynamics between rubidium atoms (Rb) and oxygen anions (O^-) are studied in a hybrid atom-ion trap. The amount of excited rubidium present in the atomic ensemble is actively controlled, providing a tool to tune the electronic quantum state of the system and, thus, the anion-neutral interaction dynamics. For a ground state Rb interacting with O^- , the detachment induced loss rate is consistent with zero, while the excited state Rb yields a significantly higher loss rate. The results are interpreted via *ab initio* potential energy curves and compared to the previously studied Rb- OH^- system, where an associative electronic detachment reactive loss process hinders the sympathetic cooling of the anion. This implies that with the loss channels closed for ground-state Rb and O^- anion, this system provides a platform to observe sympathetic cooling of an anion with an ultracold heavy buffer gas.

Published under an exclusive license by AIP Publishing. <https://doi.org/10.1063/5.0082734>

I. INTRODUCTION

Anion-neutral reactions play a key role in diverse fields ranging from organic chemistry studying S_N2 reactions^{1–3} to Earth's atmosphere^{4–6} and the interstellar medium.^{7,8} Over the last years, many techniques were developed to study anion-neutral chemistry, including flow and drift tubes,^{9–11} crossed beam apparatus,^{12–14} guided ion beams,^{15–17} and ion traps.^{18–20}

Recent developments in the field of hybrid atom-ion traps have further facilitated the study of cold and controlled ion-neutral reactions.²¹ These works demonstrate the influence of the nuclear spin configuration^{22,23} or the valence orbital on reaction rates, as well as deviations from classical capture models at low collision energies.^{24,25} With a large amount of control and tunability, these hybrid traps provide a platform for investigating the dynamics of ion-neutral systems.

A class of ion-neutral interactions unique to anionic systems are electronic detachment processes. Due to the small binding

energy of the electron, these detachment processes are frequently observed and can occur via different channels.^{26–28} One of the most extensively studied processes is the associative electronic detachment (AED) reaction.^{28–30} Here, the excess electron is detached from the reaction complex to stabilize the formation of a neutral molecule. This class of reactions is one of the main destruction mechanisms of anions in the interstellar medium and plays a relevant role as an intermediate step in the creation of other molecules.^{7,31–33}

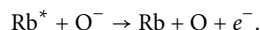
The system Rb- OH^- has been of particular interest for theoretical and experimental studies while investigating AED reactions.^{29,30,34,35} A recent comprehensive study on this system³⁶ investigates the dynamics of electronic quantum-state dependent AED reaction, where the reaction proceeds via a dipole-bound intermediate complex. In the case of an excited state rubidium, an unstable intermediate is formed, but for a ground state rubidium, this complex is stable. The probability that the reaction takes place is determined by the crossing between the anionic and neutral potential energy curves (PECs). The important implications of

these results were to identify the effective core potentials (ECPs) suitable to investigate such anion–neutral collisional dynamics and also to quantify AED reaction as the main loss channel in the Rb-OH^- system. The latter is of key consequence in determining the feasibility of sympathetic cooling of the anion via collisions with the ultracold buffer gas of laser-cooled rubidium atoms. Sympathetic cooling of atomic and molecular ions to ultracold temperatures via a neutral buffer gas has paved way for multiple areas of research particularly in cation–atom systems²¹ but is not as extensively investigated in anion–atom systems. In the Rb-OH^- system, there is a finite probability, even for Rb in its ground state to undergo AED with OH^- , making the cooling of the molecular anion rather inefficient. It can be inferred that limiting the loss from both the ground and excited state channels is crucial to observing sympathetic cooling.³⁷

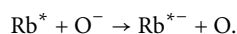
In order to study a system where the detachment loss channels are potentially suppressed, we extend our work to investigate the electronic quantum state-dependent detachment reactions between Rb atoms and O^- . With a mass ratio quite similar to Rb-OH^- , the cooling dynamics in this system will also be primarily influenced by the presence of reactive processes. Based on the electron affinity of Rb (0.49 eV³⁸) and O (1.46 eV³⁹), the only energetically possible channel for ground state rubidium interacting with O^- is the AED process where $\text{Rb} + \text{O}^- \rightarrow \text{RbO} + e^-$.

Analogous to the Rb-OH^- case, in addition to AED, several channels open for the reaction of O^- with excited state Rb, which has an energy of ~ 1.6 eV higher than Rb in its ground state. As a result, the following loss channels are also energetically accessible:

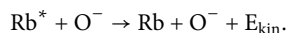
- Penning detachment (PD),



- Charge transfer (CT),



- Electronic to kinetic energy transfer (leading to loss of the ion from the trap),



Here, the loss channels PD and CT are exo-energetic, corresponding to an energy difference of $\Delta E \approx -0.14$ eV and $\Delta E \approx -0.63$ eV, respectively. For Rb-OH^- system, these channels were shown to be negligible in comparison to AED. However, these results cannot be straightforwardly extrapolated to the Rb-O^- system. In particular, the Penning detachment reaction channel, closed in the Rb-OH^- case, is an additional loss channel that will compete with AED and is likely to be comparable with the latter.²⁶ Together, all these channels contribute to the ion losses from the trap.

In this work, we experimentally investigate the electronic quantum state-dependent detachment processes between Rb atoms and O^- anions in a hybrid atom–ion trap, where the fraction of electronically excited rubidium in the atom ensemble is precisely controlled. The atom-induced ion losses are measured as a function of this excited state fraction, which yields a loss rate coefficient for ground state and excited state rubidium interacting with O^- . The possible

loss channels are discussed, and the measured experimental results are interpreted via *ab initio* potential energy surfaces describing the most relevant AED process. Finally, the implications of these results on the sympathetic cooling of O^- ions in such hybrid atom–ion traps are discussed.

II. EXPERIMENT

The experimental setup uses a hybrid atom–ion trap as shown in Fig. 1(a). The ions are produced in a plasma discharged source, from a mixture of argon gas and water vapor. The time of flight of ions depends on the mass to charge ratio and is separated in the time domain as they traverse through the Wiley–McLaren spectrometer. The ions are then mass-selected to only load the O^- ions into the octupole radio-frequency wire-trap. The multipole trap configuration provides a nearly field-free region, which decreases ion heating caused by collisions in the radio-frequency field. The use of wires in place of the conventionally used thicker cylindrical rods provides the optical access needed for cooling or diagnostic laser beams. In order to ensure stable trapping of O^- ions, a peak-to-peak radio-frequency voltage of 340 V is chosen at an angular frequency of $\omega = 2\pi \cdot 6.8$ MHz. The trapped ions are then thermalized for 200 ms with a pulse of the helium buffer gas at room temperature. The length of the buffer gas is chosen such that ions exhibit a thermal behavior in their time-of-flight distribution. The temperature of the ions is determined by mapping their temperature to their time of flight during extraction from the trap. The temperature of the ion cloud, after interaction with the helium buffer gas, is estimated to be 370(12) K. Since the time-of-flight distribution is well-described by a Gaussian distribution with no high-energy tails, we conclude that the energy distribution of the trapped ions is thermal. A more detailed description of the setup including an explanation of the used thermometry method can be found in Ref. 40. The same method is also used to measure the ion temperature after interaction with the rubidium atoms. The spatial distribution of the ions is determined via photodetachment tomography via a far-threshold laser beam.⁴¹ In the axial direction, the ions exhibit a Gaussian distribution due to the harmonic trapping potential in this direction. Radially, the spatial distribution of ions is governed by the r^6 radial potential of an octupole trap.

Once the ions are loaded in the trap and thermalized with the helium buffer gas pulse, a laser-cooled cloud of ultracold ^{85}Rb atoms is created at the center of the ion cloud. The energy level scheme is shown in Fig. 1(b). The atoms are loaded from a 2D magneto-optical trap into a dark spontaneous-force trap (darkSPOT). In this configuration, the intensity of the repumper laser beam is suppressed, thus reducing the number of atoms pumped into the cooling cycle and increasing the number of atoms in the ground state $F = 2$. Therefore, by tuning the intensity of the repumper laser beam, the number of atoms pumped into the cooling cycle can be controlled. This is quantified as the excited state fraction, defined as the ratio of number of atoms in the excited state ($F' = 4 + F' = 3$) to the total number of atoms ($F' = 4 + F' = 3 + F = 3 + F = 2$). The former is determined via fluorescence imaging and the latter is determined via saturation absorption imaging.⁴² The control on the amount of excited rubidium provides a tool to investigate the electronic state-dependent reaction dynamics of this system.

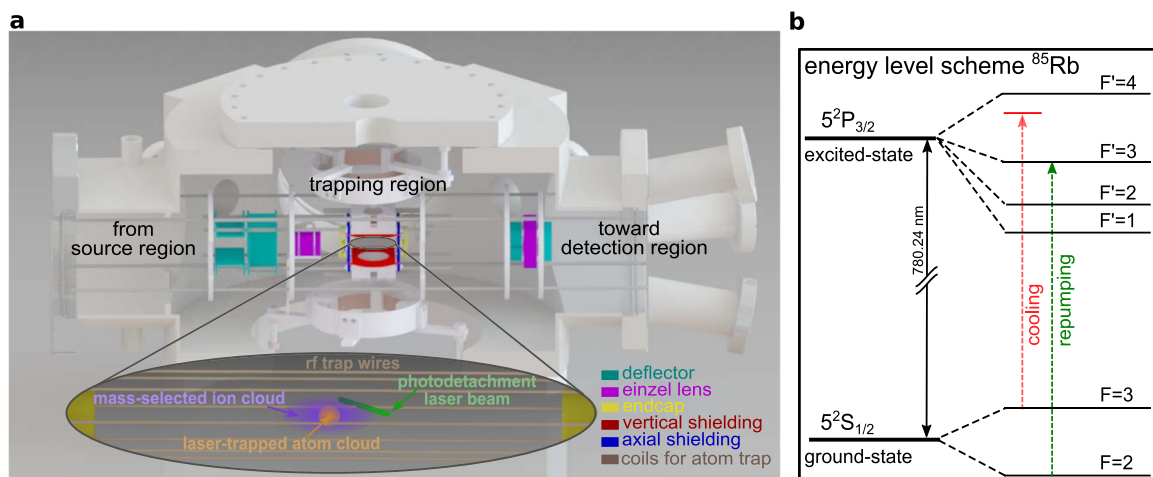


FIG. 1. (a) Hybrid atom-ion trap setup. The ions are produced in the source chamber and loaded into the radio-frequency ion trap. The trap electrodes are shown in different colors. The spatial distribution of the trapped ion cloud (purple cloud) is performed via photodetachment tomography with a far-threshold laser beam (shown in green). The ions are concentrically overlapped with a laser-cooled ^{85}Rb atom cloud (orange). After interaction with the atoms, the ions are guided toward the detector and their temperature is extracted from their time of flight to the detector. (b) Energy level scheme for ^{85}Rb . The cooling and repumper transitions are shown in red and green, respectively. In the darkSPOT configuration, the population of the state $F = 2$ is increased by spatially reducing the intensity of the repumper laser beam. This provides a tool to control the electronic state configuration of the atomic ensemble, by changing the amount of rubidium present in the excited state $5^2P_{3/2}$ or the ground state $5^2S_{1/2}$.

III. DETERMINATION OF RATE COEFFICIENTS

Once the loading of the atoms in the trap (at the center of the ion cloud) starts, the atoms and ions undergo elastic and reactive collisions. The elastic collisions transfer kinetic energy from the hotter species, resulting in the sympathetic cooling of the ions. In this case, O^- anions are cooled sympathetically via elastic collisions with ultracold rubidium. The reactive collisions result in the loss of the anions due to the formation of rubidium monoxide. The ion number and their time-of-flight distribution are recorded for different interaction times with the atom cloud. The time $t = 0$ represents the start of the loading of the atoms in the trap.

The overlap $\Phi(t)$ between the two clouds depends on their density distribution and is defined as

$$\Phi(t) = \int_0^t \rho_{\text{ion}}(x, y, z, T(t)) \rho_{\text{atom}}(x, y, z, t) dx dy dz. \quad (1)$$

Here, ρ_{atom} and ρ_{ion} are the time-dependent density distributions of the atom and ion cloud, respectively. The time-dependence of the atom cloud distribution is described as

$$\rho_{\text{atom}}(t) = \rho_{\text{atom},0} (1 - \exp(-t \cdot L)), \quad (2)$$

where $\rho_{\text{atom},0}$, the peak atom density, and L , the loading rate, are the fit parameters obtained by fitting the measured data to Eq. (2). The measured loading of the atom cloud and its corresponding fit and fit parameters are shown in Fig. 2(a). The atom density distribution is experimentally determined via saturation absorption imaging. The initial density distribution of ions (at $t = 0$) is determined via photodetachment tomography. This density distribution is dynamically altered due to elastic collisions with the atoms. As the ion temperature changes, the spatial distribution of ions also evolves accordingly. The ion temperature after interaction with the atom cloud is shown

in Fig. 2(b) (purple points). The interpolation of the ion temperature as a function of the interaction time is calculated (purple curve), representing the time-evolution of the density distribution of ions. After the time-dependent density distributions of the atom and ion cloud are estimated, the overlap is calculated via Eq. (1), and the evolution of the ion number $N_i(t)$ is described as

$$N_i(t) = N_0 \cdot \exp\left(-k \int_0^t \Phi(t') dt'\right) \exp(-k_{\text{pd}} t). \quad (3)$$

Here, N_0 is the initial number of ions at $t = 0$, k is the reactive rate coefficient, and k_{pd} is the background photodetachment loss. The photodetachment threshold of O^- (≈ 1.46 eV) is lower than that of the cooling light needed for cooling ^{85}Rb (≈ 1.6 eV). The ion loss rate due to the photodetachment of the anion is determined via an independent measurement (blue points in Fig. 2(c)), where the atoms are not loaded into the trap but the cooling (and repumping) laser beams are switched on. An exponential fit to the ion number recorded after the interaction time with these laser beams yields the photodetachment rate k_{pd} [blue curve in Fig. 2(c)]. With all these parameters pre-determined, the measured ion losses due to the varying interaction time with the atoms [red points in Fig. 2(c)] are fitted with Eq. (3) [red curve in Fig. 2(c)], yielding the reaction rate coefficient k for a given excited state fraction.

As previously mentioned, by tuning the intensity of the repumper laser beam, it is possible to vary the amount of excited rubidium in the atomic ensemble, i.e., the excited state fraction. The reaction rate coefficient, k , is determined for various excited state fractions, and the observed dependency is plotted in Fig. 3. From a linear fit (green line) through the experimentally measured data (black points), the reaction rate coefficient in the case of an excited state rubidium interacting with O^- anion is measured as $k_{\text{es}} = (1.8 \pm 0.1) \cdot 10^{-9} \text{ cm}^3 \text{ s}^{-1}$. In the case of a system with ground state

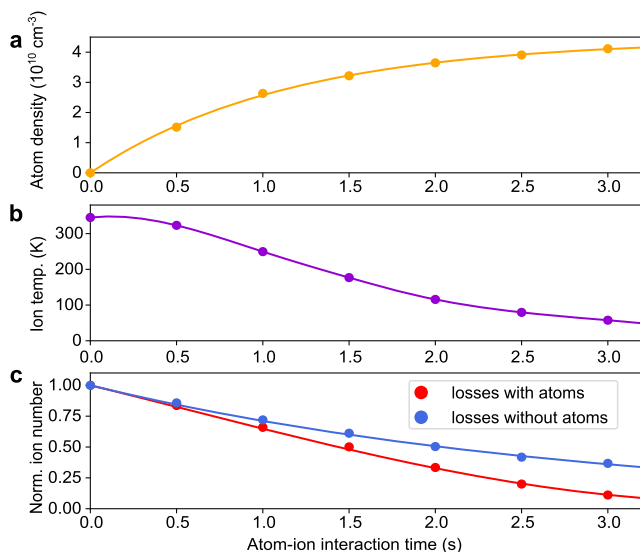


FIG. 2. Temporal evolution of atom density, ion temperature, and normalized ion number are shown. The statistical errors of the measured data (points) are smaller than their point size. (a) The measured time-evolution of the atom density is shown (orange points). This is fitted with the function in Eq. (2) yielding the atom cloud loading rate, $L = 0.87(3) \text{ s}^{-1}$, and the peak atom density, $\rho_{\text{atom},0} = 4.42(5) \cdot 10^{10} \text{ cm}^{-3}$ (orange curve). (b) The measured time-evolution of the ion temperature due to interaction with an ultracold buffer gas is shown (purple points). The interpolation function for the ion temperature as a function of the interaction time (purple curve) provides the corresponding change in the density distribution of ions. (c) The measured normalized ion losses as a function of the atom-ion interaction time. Here, the background loss rate, $k_{\text{pd}} = 0.339(6) \text{ s}^{-1}$, is determined without the presence of atoms (blue points), fitted with an exponential decay function (blue curve). For an exemplary excited state fraction of 0.113(5), the ion losses with the atoms (red points) fitted with Eq. (3) (red curve) yield the reaction rate coefficient $k = 1.95(4) \cdot 10^{-10} \text{ cm}^3 \text{ s}^{-1}$. The uncertainty due to systematic errors is estimated to be $\sim 40\%$.

rubidium, the extrapolation of the fit to zero (fit intercept) yields the reaction rate coefficient as $k_{\text{gs}} = (-0.8 \pm 3.1) \cdot 10^{-11} \text{ cm}^3 \text{ s}^{-1}$. The systematic errors are estimated at $\sim 40\%$ and attributed to the errors in the characterization of the atom cloud diagnostics via fluorescence imaging and saturation absorption imaging.

IV. INTERPRETATION

Experimental results show that the loss rate coefficient for the ground state Rb interacting with O^- is consistent with zero. As discussed earlier, the AED channel is the only energetically possible loss channel in the $\text{Rb}-\text{O}^-$ system, where Rb is in the ground state. AED reactions occur if the potential energy curves for the anionic and neutral systems cross, thus enabling a transition between the two systems. If such crossings are not energetically accessible, the detachment can only be triggered through non-adiabatic couplings,⁴³ for which the rate of electron detachment is several orders of magnitude smaller than for the former mechanism.⁴⁴

In order to confirm if such crossings are present along the ground state reaction path, the potential energy curves (PECs) that correlate with the entrance channel $\text{Rb}(^2\text{S}) + \text{O}^-$ have been

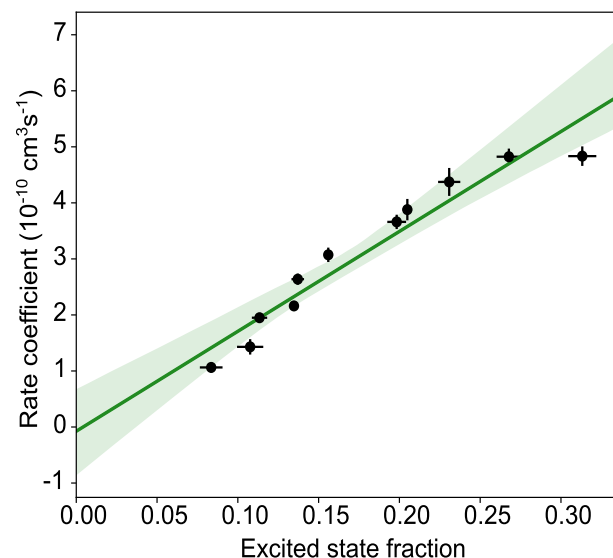


FIG. 3. Electronic state-dependent reaction dynamics. The reaction rate coefficients for different electronic configurations of the atomic ensemble are plotted as a function of the corresponding excited state fractions of the atom cloud. The experimentally measured data (black points) is fitted with a linear function (green line). The error bars of the data points represent the Gaussian propagated statistical errors. The slope (intercept) of the linear fit yields the reaction rate coefficient of O^- interacting with excited (ground) state rubidium. The green shaded region shows the 95% confidence bands of the true fit.

calculated using *ab initio* methods. All calculations have been performed with the MOLPRO program.⁴⁵ The Davidson corrected multi-reference configuration interaction with single and double (MRCISD + Q) method⁴⁶ is applied to a set of state-averaged molecular orbitals obtained using the complete active space self-consistent approach (CASSCF). The active space includes 6 σ and 2 π orbitals, corresponding to valence orbitals and inner-valence shells of the Rb atom (4s and 4p orbitals). The multiconfiguration Dirac-Fock (MDF) electron core potential and the corresponding *spdf* segmented valence basis set,⁴⁷ augmented by a set of 3s, 2p, and 1d even-tempered diffuse functions, have been used to describe the 28 core electrons and the 9 outer electrons of Rb, respectively. The oxygen atom has been described by the quadruple zeta augmented valence correlation-consistent Dunning basis sets⁴⁸ (AVQZ). The calculated PECs are depicted in Fig. 4. The main panel shows the four molecular RbO^- states that correlate with the ground state entrance channel $\text{Rb}(^2\text{S}) + \text{O}^-$: $^1\Sigma^+$, $^3\Sigma^+$, $^1\Pi$, and $^3\Pi$. Their energy ordering follows the trend seen in other alkali oxides.^{49,50} All anionic states are valence bound states that are all stable against autodetachment, i.e., their respective detachment energies (energy gap between anion and neutral PECs at their respective minimum) are positive. This is predicted to be about 1.2 eV, as compared to about 0.3 eV for the case of $\text{Rb}-\text{OH}^-$,³⁰ and the AED reaction is predicted to be exo-energetic ($\Delta E \approx -1.1 \text{ eV}$). In addition, no crossing between anion and neutral PECs can be seen along the reaction path. Due to the large reduced mass and rather large detachment energies, the non-adiabatic detachment rate is expected to be orders of magnitude smaller than the Langevin rate of $4.4 \cdot 10^{-9} \text{ cm}^3 \text{ s}^{-1}$.⁵¹ This is in

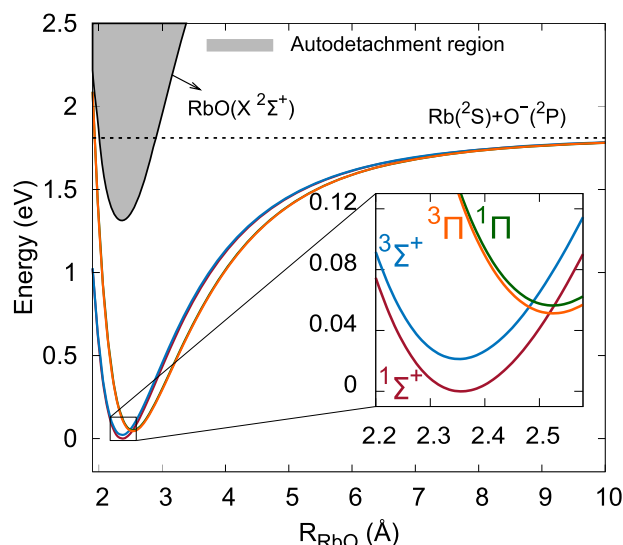


FIG. 4. The main panel shows the potential energy curves (PECs) describing the four molecular states that correlate with the $\text{Rb}(^2\text{S}) + \text{O}^-(^2\text{P})$ ground state channel (colored lines) and the neutral ground state RbO (black line). The smaller inset shows the anion PECs around the potential well. The dashed line corresponds to the energy at the ground state entrance channel.

agreement with the previously determined negligible rate coefficient for the ground state.

The collisions of O^- with excited Rb lead to losses with a measured rate coefficient of $k_{\text{es}} = (1.8 \pm 0.1) \cdot 10^{-9} \text{ cm}^3 \text{ s}^{-1}$. Even considering the systematic error of 40%, this value is significantly lower than the Langevin rate of $7.4 \cdot 10^{-9} \text{ cm}^3 \text{ s}^{-1}$. Such a discrepancy was also observed in the previous work investigating the $\text{Rb}-\text{OH}^-$ case.³⁶ These results indicate the presence of other processes in the system, which suppress the coupling into the autodetachment manifold. The reduced loss rate from the excited channel could be explained by the presence of higher-lying excited states that are stable against autodetachment, thus providing reaction paths that avoid the loss channels. In addition, some dynamical stabilization processes may occur, leading to non-unity detachment probability when the autodetachment region is reached. This could result in an overall reduced loss rate. A thorough theoretical investigation of the stability of the higher-lying excited states against autodetachment is needed to quantitatively explain the observed deviation for the excited state.

V. CONCLUSION

We have measured electronic quantum state-dependent loss rates in a hybrid ion-atom trap involving ultracold Rb atoms and trapped O^- anions. The energetically allowed electron detachment processes are identified as associative electronic detachment (AED) for the ground state $\text{Rb}(^2\text{S}) + \text{O}^-$ channel and AED, charge-transfer, and Penning detachment for the excited state $\text{Rb}(^2\text{P}) + \text{O}^-$ channel. A detailed theoretical description of the structure, dynamics, and stability of the excited state of the $\text{Rb}-\text{O}^-$ system and an experimental framework to distinguish these different loss channels is required. In this work, we observed a vanishingly small loss rate for

the reaction with Rb in its ground state. The potential energy curves are calculated using *ab initio* methods. The AED channel is predicted to be exo-energetic. However, all anionic states are found to be stable against autodetachment, and no crossings into the autodetachment region are seen, supporting the experimentally observed vanishing rate coefficient. For reactions involving excited Rb, a rate significantly lower than the Langevin rate is observed, indicating the presence of dynamical stabilization processes. This discrepancy is similar to the one observed in the $\text{Rb}-\text{OH}^-$ case.

From the results obtained for the ground state rate coefficient, it can be inferred that it is possible to minimize the O^- ion losses by confining rubidium atoms only in their ground state, for example, in a dipole trap. Additionally, a far-detuned dipole trap would also suppress photodetachment losses, which would result in a higher number of elastic collisions, resulting in a more efficient sympathetic cooling of the ions.

Besides the atom-to-ion mass ratio, the key properties that govern the dynamics of ion sympathetic cooling in the trap are the ion-ion thermalization rate, the atom-ion elastic collision rate, and the atom-ion reactive collision rate. The ratio of atom-ion elastic to reactive collision rate is critical in determining the cooling efficiency.^{52,53} Considering the measured loss rate, this elastic to reactive collision ratio is estimated to be an order of magnitude larger in the $\text{Rb}-\text{O}^-$ system as opposed to the $\text{Rb}-\text{OH}^-$ system,³⁶ making it feasible to observe anion sympathetic cooling in this system. The first signatures of anion sympathetic cooling are already seen in this work [see Fig. 2(b)] and will be further investigated in the future.

ACKNOWLEDGMENTS

We acknowledge the support from the Austrian Science Fund (FWF) under Project No. I3159-N36 and Deutsche Forschungsgemeinschaft (DFG) under Project No. WE/2661/14-1. S.Z.H. acknowledges the support from the HGSFP fellowship. M.K. is grateful to the BMBF project MeSoX (Project No. 05K19GUE) for financial support.

AUTHOR DECLARATIONS

Conflict of Interest

The authors have no conflicts to disclose.

DATA AVAILABILITY

The data that support the findings of this study are available from the corresponding author upon reasonable request.

REFERENCES

- 1 M. L. Chabiny, S. L. Craig, C. K. Regan, and J. I. Brauman, "Gas-phase ionic reactions: Dynamics and mechanism of nucleophilic displacements," *Science* **279**, 1882–1886 (1998).
- 2 S. Schmatz, "Quantum dynamics of gas-phase $\text{S}_\text{N}2$ reactions," *ChemPhysChem* **5**, 600–617 (2004).
- 3 J. Mikosch, S. Trippel, C. Eichhorn, R. Otto, U. Lourderaj, J. X. Zhang, W. L. Hase, M. Weidemüller, and R. Wester, "Imaging nucleophilic substitution dynamics," *Science* **319**, 183–186 (2008).

- ⁴S. G. Ard, J. J. Melko, B. Jiang, Y. Li, N. S. Shuman, H. Guo, and A. A. Viggiano, "Temperature dependences for the reactions of O_2^- and O^- with N and O atoms in a selected-ion flow tube instrument," *J. Chem. Phys.* **139**, 144302 (2013).
- ⁵N. S. Shuman, D. E. Hunton, and A. A. Viggiano, "Ambient and modified atmospheric ion chemistry: From top to bottom," *Chem. Rev.* **115**, 4542–4570 (2015).
- ⁶M. S. Ugelow, J. L. Berry, E. C. Browne, and M. A. Tolbert, "The impact of molecular oxygen on anion composition in a hazy Archean earth atmosphere," *Astrobiology* **20**, 658–669 (2020).
- ⁷T. J. Millar, C. Walsh, and T. A. Field, "Negative ions in space," *Chem. Rev.* **117**, 1765–1795 (2017).
- ⁸E. Yurtsever, M. Satta, R. Wester, and F. A. Gianturco, "On the formation of interstellar CH^- anions: Exploring mechanism and rates for CH_2 reacting with H^- ," *J. Phys. Chem. A* **124**, 5098–5108 (2020).
- ⁹C. H. DePuy, J. J. Grabowski, and V. M. Bierbaum, "Chemical reactions of anions in the gas phase," *Science* **218**, 955–960 (1982).
- ¹⁰A. A. Viggiano, R. A. Morris, J. S. Paschkewitz, and J. F. Paulson, "Kinetics of the gas-phase reactions of Cl^- with CH_3Br and CD_3Br : Experimental evidence for nonstatistical behavior?," *J. Am. Chem. Soc.* **114**, 10477–10482 (1992).
- ¹¹V. M. Bierbaum, "Go with the flow: Fifty years of innovation and ion chemistry using the flowing afterglow," *Int. J. Mass Spectrom.* **377**, 456–466 (2015).
- ¹²R. L. Champion, L. D. Doverspike, M. S. Huq, D. Scott, and Y. Wang, "Reactive scattering and electron detachment for collisions of halogen negative ions with HCl , DCl , and HBr ," *J. Chem. Phys.* **88**, 5475–5480 (1988).
- ¹³M. A. Huels, R. L. Champion, L. D. Doverspike, and Y. Wang, "Charge transfer and electron detachment for collisions of H^- and D^- with H_2 ," *Phys. Rev. A* **41**, 4809–4815 (1990).
- ¹⁴S. Živanov, M. Čížek, J. Horáček, and M. Allan, "Electron spectra for associative detachment in low-energy collisions of Cl^- and Br^- with H and D ," *J. Phys. B: At., Mol. Opt. Phys.* **36**, 3513–3531 (2003).
- ¹⁵E. Haufler, S. Schlemmer, and D. Gerlich, "Absolute integral and differential cross sections for the reactive scattering of $\text{H}^- + \text{D}_2$ and $\text{D}^- + \text{H}_2$," *J. Phys. Chem. A* **101**, 6441–6447 (1997).
- ¹⁶K. Rempala and K. M. Ervin, "Collisional activation of the endoergic hydrogen atom transfer reaction $\text{S}^-(^2\text{P}) + \text{H}_2 \rightarrow \text{SH}^- + \text{H}$," *J. Chem. Phys.* **112**, 4579–4590 (2000).
- ¹⁷L. A. Angel, M. K. Dogbevia, K. M. Rempala, and K. M. Ervin, "Gas-phase hydrogen atom abstraction reactions of S^- with H_2 , CH_4 , and C_2H_6 ," *J. Chem. Phys.* **119**, 8996–9007 (2003).
- ¹⁸D. Gerlich, "Ion-neutral collisions in a 22-pole trap at very low energies," *Phys. Scr.* **1995**, 256–263.
- ¹⁹R. Wester, "TUTORIAL: Radiofrequency multipole traps: Tools for spectroscopy and dynamics of cold molecular ions," *J. Phys. B: At., Mol. Opt. Phys.* **42**, 154001 (2009).
- ²⁰D. Hauser, S. Lee, F. Carelli, S. Spieler, O. Lakhmanskaya, E. S. Endres, S. S. Kumar, F. Gianturco, and R. Wester, "Rotational state-changing cold collisions of hydroxyl ions with helium," *Nat. Phys.* **11**, 467–470 (2015).
- ²¹M. Tomza, K. Jachymski, R. Gerritsma, A. Negretti, T. Calarco, Z. Idziaszek, and P. S. Julienne, "Cold hybrid ion-atom systems," *Rev. Mod. Phys.* **91**, 035001 (2019).
- ²²A. Kilaj, H. Gao, D. Röscher, U. Rivero, J. Küpper, and S. Willitsch, "Observation of different reactivities of *para* and *ortho*-water towards trapped diazenylium ions," *Nat. Commun.* **9**, 2096 (2018).
- ²³T. Sikorsky, Z. Meir, R. Ben-Shlomi, N. Akerman, and R. Ozeri, "Spin-controlled atom-ion chemistry," *Nat. Commun.* **9**, 920 (2018).
- ²⁴F. H. J. Hall and S. Willitsch, "Millikelvin reactive collisions between sympathetically cooled molecular ions and laser-cooled atoms in an ion-atom hybrid trap," *Phys. Rev. Lett.* **109**, 233202 (2012).
- ²⁵P. Puri, M. Mills, I. Simbotin, J. A. Montgomery, R. Côté, C. Schneider, A. G. Suits, and E. R. Hudson, "Reaction blockading in a reaction between an excited atom and a charged molecule at low collision energy," *Nat. Chem.* **11**, 615–621 (2019).
- ²⁶R. S. Berry, "Odyssey and oddity: Photo- and collision processes you would not expect," *Phys. Chem. Chem. Phys.* **7**, 286–290 (2005).
- ²⁷A. Midey, I. Dotan, J. V. Seeley, and A. A. Viggiano, "Reactions of small negative ions with $\text{O}_2(\text{a } ^1\Delta_g)$ and $\text{O}_2(\text{X}^3\Sigma^-_g)$," *Int. J. Mass Spectrom.* **280**, 6–11 (2009).
- ²⁸H. Bruhns, H. Kreckel, K. Miller, M. Lestinsky, B. Seredyuk, W. Mitthumsiri, B. L. Schmitt, M. Schnell, X. Urbain, M. L. Rappaport, C. C. Havener, and D. W. Savin, "A novel merged beams apparatus to study anion-neutral reactions," *Rev. Sci. Instrum.* **81**, 013112 (2010).
- ²⁹J. N. Byrd, H. H. Michels, J. A. Montgomery, and R. Côté, "Associative detachment of rubidium hydroxide," *Phys. Rev. A* **88**, 032710 (2013).
- ³⁰M. Kas, J. Loreau, J. Liévin, and N. Vaeck, "Ab initio study of the neutral and anionic alkali and alkaline earth hydroxides: Electronic structure and prospects for sympathetic cooling of OH^- ," *J. Chem. Phys.* **146**, 194309 (2017).
- ³¹J. L. Moruzzi, J. W. Ekin, and A. V. Phelps, "Electron production by associative detachment of O^- ions with NO , CO , and H_2 ," *J. Chem. Phys.* **48**, 3070–3076 (1968).
- ³²H. Kreckel, H. Bruhns, M. Cizek, S. C. Glover, K. A. Miller, X. Urbain, and D. W. Savin, "Experimental results for H_2 formation from H^- and H and implications for first star formation," *AIP Conf. Proc.* **1642**, 388–391 (2015).
- ³³R. Plašil, T. D. Tran, Š. Roučka, P. Jusko, D. Mulin, I. Zymak, S. Rednyk, A. Kovalenko, P. Dohnal, J. Glosik, K. Houfek, J. Táborský, and M. Čížek, "Isotopic effects in the interaction of O^- with D_2 and H_2 at low temperatures," *Phys. Rev. A* **96**, 062703 (2017).
- ³⁴M. Kas, J. Loreau, J. Liévin, and N. Vaeck, "Ab initio study of reactive collisions between $\text{Rb}(^2\text{S})$ or $\text{Rb}(^2\text{P})$ and $\text{OH}^-(^1\Sigma^+)$," *J. Chem. Phys.* **144**, 204306 (2016).
- ³⁵J. Deiglmayr, A. Göritz, T. Best, M. Weidemüller, and R. Wester, "Reactive collisions of trapped anions with ultracold atoms," *Phys. Rev. A* **86**, 043438 (2012).
- ³⁶S. Z. Hassan, J. Tauch, M. Kas, M. Nötzold, H. López-Carrera, E. S. Endres, R. Wester, and M. Weidemüller, "Associative detachment in anion-atom reactions involving a dipole-bound electron," *Nat. Commun.* **13**, 818 (2022).
- ³⁷M. Kas, J. Loreau, J. Liévin, and N. Vaeck, "Cold reactive and nonreactive collisions of Li and Rb with C_2^- : Implications for hybrid-trap experiments," *Phys. Rev. A* **99**, 042702 (2019).
- ³⁸P. Frey, F. Breyer, and H. Holop, "High resolution photodetachment from the rubidium negative ion around the $\text{Rb}(5p_{1/2})$ threshold," *J. Phys. B: At. Mol. Phys.* **11**, L589–L594 (1978).
- ³⁹S. J. Cavanagh, S. T. Gibson, M. N. Gale, C. J. Dedman, E. H. Roberts, and B. R. Lewis, "High-resolution velocity-map-imaging photoelectron spectroscopy of the O^- photodetachment fine-structure transitions," *Phys. Rev. A* **76**, 052708 (2007).
- ⁴⁰M. Nötzold, S. Z. Hassan, J. Tauch, E. Endres, R. Wester, and M. Weidemüller, "Thermometry in a multipole ion trap," *Appl. Sci.* **10**, 5264 (2020).
- ⁴¹P. Hlavenka, R. Otto, S. Trippel, J. Mikosch, M. Weidemüller, and R. Wester, "Absolute photodetachment cross section measurements of the O^- and OH^- anion," *J. Chem. Phys.* **130**, 061105 (2009).
- ⁴²B. Höltschmeier, J. Gläsel, H. López-Carrera, and M. Weidemüller, "A dense gas of laser-cooled atoms for hybrid atom-ion trapping," *Appl. Phys. B* **123**, 51 (2017).
- ⁴³M. Čížek, J. Dvořák, and K. Houfek, "Associative detachment in $\text{Li} + \text{H}^-$ collisions," *Eur. Phys. J. D* **72**, 66 (2018).
- ⁴⁴J. Simons, "Theoretical study of negative molecular ions," *Annu. Rev. Phys. Chem.* **62**, 107–128 (2011).
- ⁴⁵H. Werner, P. J. Knowles, G. Knizia, F. R. Manby, M. Schütz, P. Celani, T. Korona, R. Lindh, A. Mitrushenkov, G. Rauhut, K. R. Shamasundar, T. B. Adler, R. D. Amos, A. Bernhardsson, A. Berning, D. L. Cooper, M. J. O. Deegan, A. J. Dobbyn, F. Eckert, E. Goll, C. Hampel, A. Hesselmann, G. Hetzer, T. Hrenar, G. Jansen, C. Köppl, Y. Liu, A. W. Lloyd, R. A. Mata, A. J. May, S. J. McNicholas, W. Meyer, M. E. Mura, A. Nicklass, D. P. O'Neill, P. Palmieri, D. Peng, K. Pflüger, R. Pitzer, M. Reiher, T. Shiozaki, H. Stoll, A. J. Stone, R. Tarroni, T. Thorsteinsson, and M. Wang, MOLPRO, version 2012.1, a package of *ab initio* programs, 2012.
- ⁴⁶P. J. Knowles and H.-J. Werner, "Internally contracted multiconfiguration-reference configuration interaction calculations for excited states," *Theor. Chim. Acta* **84**, 95–103 (1992).
- ⁴⁷I. S. Lim, P. Schwerdtfeger, B. Metz, and H. Stoll, "All-electron and relativistic pseudopotential studies for the group 1 element polarizabilities from K to element 119," *J. Chem. Phys.* **122**, 104103 (2005).

- ⁴⁸T. H. Dunning, "Gaussian basis sets for use in correlated molecular calculations. I. The atoms boron through neon and hydrogen," *J. Chem. Phys.* **90**, 1007 (1989).
- ⁴⁹B. Mintz, B. Chan, M. B. Sullivan, T. Buesgen, A. P. Scott, S. R. Kass, L. Radom, and A. K. Wilson, "Structures and thermochemistry of the alkali metal monoxide anions, monoxide radicals, and hydroxides," *J. Phys. Chem. A* **113**, 9501–9510 (2009).
- ⁵⁰C. W. Bauschlicher, H. Partridge, and L. G. M. Pettersson, "Franck-Condon factors for photodetachment from LiO^- , NaO^- , and KO^- ," *J. Chem. Phys.* **99**, 3654–3658 (1993).
- ⁵¹P. Langevin, "A fundamental formula of kinetic theory," *Ann. Chim. Phys.* **5**, 245–288 (1905).
- ⁵²B. Höltkemeier, P. Weckesser, H. López-Carrera, and M. Weidemüller, "Buffer-gas cooling of a single ion in a multipole radio frequency trap beyond the critical mass ratio," *Phys. Rev. Lett.* **116**, 233003 (2016).
- ⁵³B. Höltkemeier, P. Weckesser, H. López-Carrera, and M. Weidemüller, "Dynamics of a single trapped ion immersed in a buffer gas," *Phys. Rev. A* **94**, 062703 (2016).